Biological Electron-Transfer Dynamics in Multiheme Cytochrome Complexes

Section i.

At heart, my greatest academic pleasure is learning about different cultures and their languages, histories and cultural errata. As such it seems kind of odd that I would choose to do a rigorously scientific project such as this. Nonetheless, I should first elaborate. My favorite part of learning history and about different cultures is the fact that I can synthesize a variety of different areas into one full context. I can see the interplay between different languages and how they develop along political and natural borders. As such, this project actually greatly appealed to me. I started on the foundations of the project the summer after my sophomore year in high school, fresh out of AP Calculus AB and AP Biology. While I had generally done well in the former, the latter was essentially the bane of my school year. I did not enjoy taking bio at all. However, once the summer started, I was introduced to Professor Moh El-Naggar at the NanoBio Institute at USC in order to do an internship about a bacterium. To be completely honest, I was very apprehensive about the internship, as it involved lab and experimental work in a discipline that I didn't have great experiences in. However, my attitude changed once I got a good idea of what was going on in the lab. Specifically, I was struck by the lab's outside collaborations, especially in computer science and simulations. Now, for the record, I am incredibly interested in computer science, and computers in general, to the extent that I am considering it as my major alongside linguistics, which brings in my love of the humanities. So, with this interest in mind, I was completely blown away by the fact that this bacteria research wasn't localized to just the bio lab. Once I realized that yes, it was rather impossible to analyze the energy-conversion mechanisms in bacteria with a microscope and that yes, it was more intuitive to use computers to simulate these mechanisms, I was enraptured. Scientific research had pressed the right buttons to stimulate my love of

interdisciplinary synthesis, much as linguistics and history had together. And from there, my project grew and grew in scale, incorporating a variety of different disciplines, specifically biology, physics, chemistry, mathematics, and computer science. So yes, I still do style myself a humanities person. However, this venture into hard scientific research was actually one of the most influential experiences to my life, as it opened up pathways that I had never seen before into science and the combination of disciplines.

Section ii.

Abstract

Electron transfer (ET) governs all known energy-conversion processes in biology. A remarkable example is the recent discovery of rapid ET along electrically conducting bacterial nanowires produced by *Shewanella oneidensis* MR-1. The outer-membrane cytochromes, MtrF and OmcA, are hypothesized media for ET, but how these multiheme cytochromes are assembled into a conducting complex remains a mystery. I solved this mystery by constructing an entire scientific workflow that integrates mathematical modeling, biophysics, electrochemistry, computing, and entertainment technology. Specifically, I determined the structure of MtrF-OmcA complex and study ET dynamics in it by combining homology modeling, protein docking, geometrical/biological screening, and kinetic Monte Carlo simulation. For visualizing the simulated ET dynamics with enhanced depth perception, I further built an immersive visualization system using a commodity virtual-reality platform and a game engine. My immersive simulation results reveal novel nonequilibrium phase transitions with which *Shewanella* efficiently responds to a change in its electrochemical environment. These results shed useful light on boosting the efficiency of *Shewanella*-based microbial fuel cells by increasing the ET rate, in order to produce electricity and water from sewage toward solving the global energy and environmental problems.

1. Introduction

Reduction and oxidation reactions govern a variety of biological energy-conversion processes, including respiration. Electron transfer (ET) within and across biological molecules is the key process that essentially dictates these redox reactions.[1] Such biological ET reactions have been studied extensively in the past.[2-5] A remarkable example is the rapid ET from metal reducing bacteria such as *Shewanella oneidensis* MR-1 to extracellular metal oxides that serve as terminal electron acceptors for anaerobic respiration.[6-9] Under certain conditions, *S. oneidensis* MR-1 produces electrically conductive bacterial nanowires that may mediate long-distance ET to extracellular oxidants.[10-12] A recent study has revealed that these *Shewanella* nanowires are membrane extensions decorated with the multiheme cytochromes MtrC and OmcA (Fig. 1a).[13] These molecules had been previously identified as outer-membrane cytochromes and implicated as the terminal bacterial reductases of extracellular electron acceptors.[14-17] MtrC can associate with

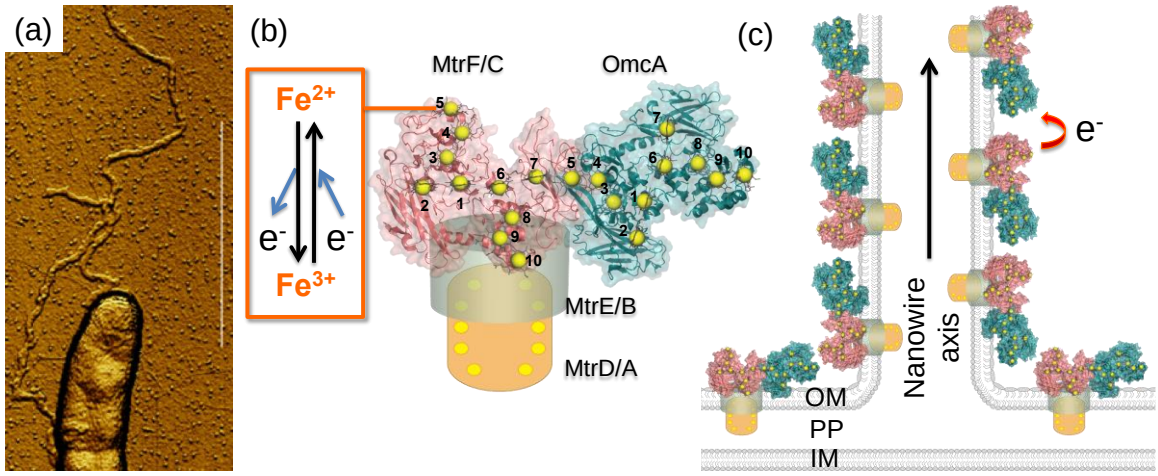

Fig. 1. (a) Atomic force microscope (AFM) image of a *Shewanella oneidensis* MR-1 cell and attached bacterial nanowires. The scale bar is 1 μm. (b) Structural model of an outer-membrane Mtr-Omc complex, where each yellow dot represents a heme group. Numerals show the numbering of the 10 hemes for both MtrC/F and OmcA. The inset shows that, in an oxidation reaction, ejection of an electron (e^-) converts the iron atom in a heme group from Fe^{2+} to Fe^{3+}, whereas, in a reduction reaction, injection of e^- converts it from Fe^{3+} to Fe^{2+}. (c) Hypothetical model of a bacterial nanowire, in which a lattice of Mtr-Omc complexes mediates long-distance electron transfer. The figure shows a central slice of the nanowire (IM: inner membrane, PP: periplasm, OM:outer membrane).

OmcA, in addition to forming a complex with the periplasmic decaheme cytochrome MtrA

through transmembrane porin MtrB; this proposed arrangement has been described as the MtrCAB porin-cytochrome conduit, allowing ET across the cell envelope.[17, 18] *Shewanella* can also express the MtrFDE conduit, which is homologous to MtrCAB, and MtrF (homolog of MtrC) has been shown to act as a terminal reductase in the absence of MtrC.[19]

The localization of MtrC and OmcA along bacterial nanowires suggests that an outer-membrane lattice of cytochrome complexes may mediate ET over micrometer length scales, as schematized in Figs. 1b and 1c.[13] Here, each complex is comprised of two decaheme cytochromes, MtrC and OmcA, each of which contains 10 hemes (Fig. 1b). The iron (Fe) atom in each heme can exist in either of the two valence states, Fe^{2+} or Fe^{3+}. Conversion of the irons between Fe^{2+} and Fe^{3+} allows for the hopping of electrons between the hemes as shown in the inset of Fig. 1b. Despite this plausible hypothesis, however, the microscopic nature of ET dynamics along these bacterial nanowires remains elusive.

Visualizing ET dynamics could provide key insight into understanding these fundamental processes and possibly controlling them for a wide range of applications including renewable energy and wastewater treatment.[20] Balabin *et al*. developed a plugin to the Visual Molecular Dynamics (VMD) software[21] that visualizes ET pathways in biomolecules based on a network model called Pathways.[22] Byun *et al*.[23] simulated the net electron flux through MtrF using, as input, the sequential heme-to-heme ET rates computed by Breuer *et al.*[24] The latter were calculated from simulations of thermodynamic and electronic coupling parameters using molecular dynamics, fragment-orbital density functional theory (similar to divide-and-conquer density functional theory, DCDFT[25]), and the quantum mechanics/molecular mechanics (QM/MM) method.[26, 27] The sequential heme-to-heme ET rates were recombined in kinetic Monte Carlo (KMC) simulations[28-31] to synthesize the global ET dynamics of MtrF.[23] These divide-conquer-recombine KMC (DCR-

KMC) simulation results were visualized using VMD, but the visualization was limited to static snapshots.

To provide better insight into the dynamics of biological ET processes, we have developed a computational framework named VizBET.[32] The framework consists of an entire workflow of the KMC simulation, and it animates the resulting ET dynamics using a new plugin to VMD. However, the user's ability to understand complex ET pathways was severely limited due to 2-dimensional (2D) rendering on traditional computer monitors. Virtual reality (VR) technologies immerse the user within three-dimensional (3D) models and allow them to navigate through the environment.[33] This type of immersive experience provides the user with the necessary perceptive depth to enhance their understanding of the ET processes being rendered. The head mounted display (HMD) is one of the earliest VR technologies, starting with an early effort by Ivan Sutherland in 1960s.[34] Currently, there is a resurgence of interest in the HMD technologies with the advent of low-cost commodity HMDs such as the Oculus Rift.[35] Thus far, however, applications for devices like the Rift have largely been limited to computer games. Reports on biomolecular visualization using the Rift are scarce,[36] and we have not found any description of general procedures for scientists to export their visual models from standard biomolecular visualization software such as VMD to the Oculus platform. To provide a more accurate representation with enhanced depth perception, we have developed an extension of VizBET named iBET to render the VMD model of ET dynamics in a commodity VR platform.[37] The iBET exports VMD models into the Unity game engine and render it in an Oculus Rift head mounted display.

This report presents key features and implementation details of VizBET/iBET, organized as follows. Section 2 describes the overall computational framework. Visual simulation results, leading to a scientific discovery, are presented in section 3, and section 4 contains a summary.

2. Methods

Figure 2a summarizes the overall workflow of the VizBET framework, using an outer-membrane MtrF-OmcA cytochrome complex in *Shewanella oneidensis* MR-1 as an example (the crystal structure of MtrC is not yet available, so the homologous MtrF was used instead). The structures of the MtrF and OmcA molecules determined by X-ray diffraction are downloaded from the protein data bank (PDB).[38] We first pre-process the PDB files to account for residues that were not resolved in the crystal structure with the aid of the homology-modeling Web server, I-TASSER.[39] The structural outputs from this pre-processing step are used as inputs to molecular-

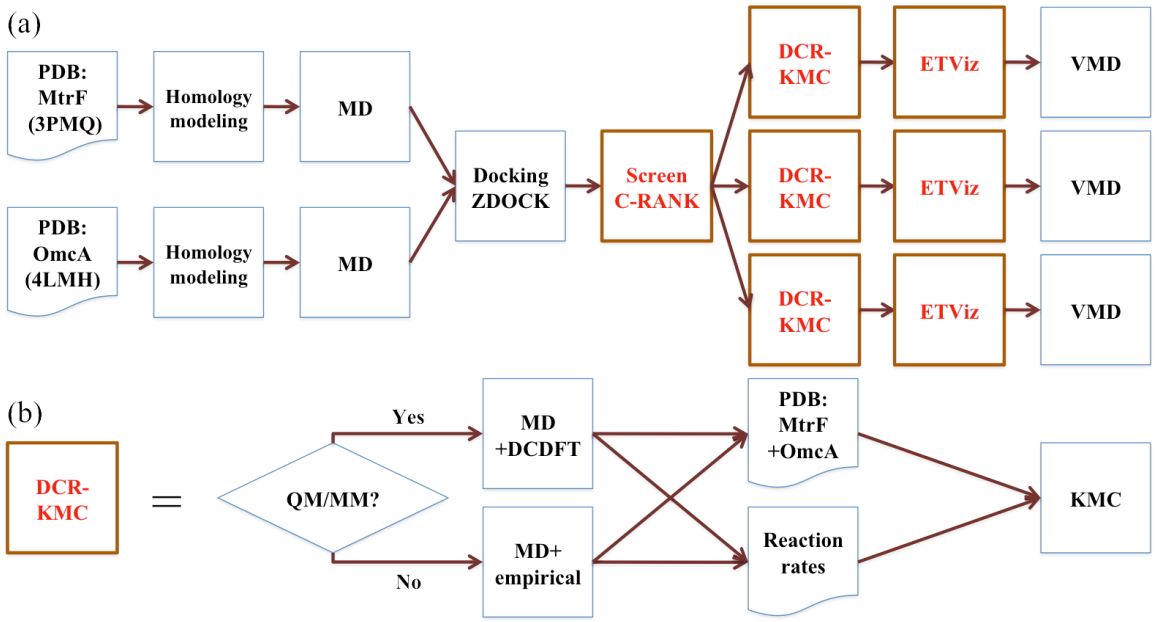

Fig. 2. (a) Workflow of the VizBET framework for biological ET visualization. Major new components developed for VizBET are represented by squares with thick lines. C-Rank consists of the further screening of ZDOCK results, MD re-solvation, and MM-PBSA. (b) Detailed workflow of the DCR-KMC (divide-conquer-recombine kinetic Monte Carlo) simulation component. QM/MM: quantum mechanics/molecular mechanics; DCDFT: divide-and-conquer density functional theory.

dynamics (MD) simulations that follow the trajectories of all atoms by numerically integrating Newton's equations of motion. Two MD simulations are performed for MtrF and OmcA molecules, respectively, in water. Individual MtrF and OmcA configurations taken from the MD simulations are used as inputs to a protein-docking program, ZDOCK,[40] to predict the structure of

the MtrF-OmcA complex. ZDOCK typically returns 2000 top configurations according to simple electrostatic and shape criteria. We have developed a C-RANK program to screen these configurations into a small subset of biologically plausible configurations, according to structural and ET criteria detailed below. Moreover, C-RANK serves as the starting point to further screen complex candidates by combining MD simulations, which re-solvate and relax the rigidly docked MtrF-OmcA complex structure, and the efficient binding free energy estimation with the method of MM/PBSA, which post-processes an ensemble of configurations from the MD trajectory with a combination of a force field and continuum solvent model.[41-44] The next step in VizBET is to perform DCR-KMC simulations for studying the ET dynamics in the selected MtrF-OmcA configurations. The DCR-KMC simulation component (Fig. 2b) within VizBET combines (1) either DCDFT or empirical approaches to compute the ET rates in a DC fashion, which are then used in (2) KMC simulations of global ET dynamics in the entire complex. We have also developed a plugin to the VMD software named ETViz to animate ET dynamics in the DCR-KMC simulations. The iBET framework enhances the perceptual depth over that of VizBET by exporting the visual output from ETViz into VR instead of a 2D computer monitor (Fig. 3).

Currently, VizBET is implemented using the bash scripting language[45] to be used with the portable batch system (PBS) for job scheduling on a Linux cluster.[46] On high-end parallel supercomputers, we can alternatively use the Swift/T parallel scripting language for efficient distributed-memory workflow processing.[47] On a Grid of distributed parallel computers, the VizBET

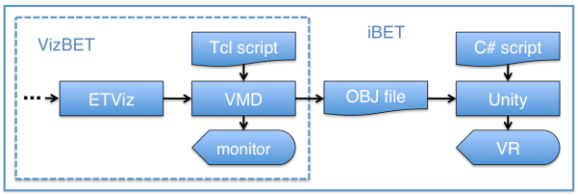

Fig. 3. Workflow of the iBET framework for immersive visualization. The original VizBET framework is enclosed by the dashed lines, in which only the final stage (*i.e.*, the ETViz visualization module) is shown.

workflow can be converted to a directed acyclic graph to be executed using a scientific workflow management system such as Pegasus.[48]

2.1. Structural modeling and molecular dynamics simulations of protein complexes

The first step is to establish homology models for both proteins (MtrF and OmcA). We initially obtain X-ray structures of MtrF and OmcA as determined from the PDB server.[49] The PDB codes for MtrF and OmcA are 3PMQ[50] and 4LMH,[51] respectively. It should be noted that hydrogen atoms are not included in these X-ray structures. In addition, certain residues located near the N- and C-termini were not resolved in the crystal structures, likely due to the flexibility of these regions. The unresolved C-terminus residues from the X-ray studies were not included in our homology models, since they result from the purification tag of the recombinant protein used for these studies. The signal peptide sequence preceding the cysteine residue of the N-terminal's LXXC cleavage and lipidation motif was also omitted from the homology model, since our goal is to study the mature proteins after cleavage and lipidation of the cysteine, which allows the anchoring of the lipoprotein to the membrane. As a result, our homology models target the amino-acid sequences of the membrane-bound forms of both proteins, starting with the cysteines. This leaves 25 and 16 N-terminus unresolved residues for MtrF and OmcA, respectively. In order to build a protein homology model by preserving the original crystal structure and the heme groups' positions while adding the missing residues, we adopt the following strategy. First, we predict the homology models of MtrF and OmcA by using the I-TASSER server[39] with each protein's sequence and its original crystal structure as a reference. Here, the predicted homology models do not include heme groups and the coordinated calcium ions (Ca^{2+}). Second, the predicted structure of the homology model is superimposed on the original crystal structure so as to minimize the mean square displacement of all non-hydrogen atoms between the two structures using least-square fitting.[52]

Third, the new residues from the optimal superposition are transferred and bonded onto the original crystal structure for each individual protein, in such a way that the heme groups and the coordinated calcium ions present in the original PDB files (one Ca^{2+} ion in 3PMQ; two Ca^{2+} ions in 4LMH) can be preserved at their original positions.

The second step is to establish both proteins' solvation structures. With the established homology models of the mature proteins, hydrogen atoms are explicitly added to both proteins. All of the amino acids are protonated (histidine (His) is treated neutral) with the exception of glutamic acid (Glu) and aspartic acid (Asp), which are taken as deprotonated. The N-terminus (NH_3^+) and the C-terminus (COO^-) are assigned with charges of +e and -e respectively. These assignments result in a net charge of -37e and -31e, respectively, for MtrF and OmcA including heme groups at pH 7. We perform MD simulations of individual MtrF and OmcA using the Gromacs software package (version 4.6.5)[53] and the Charmm 27 force-field parameters.[54] In both proteins, each Fe ion in a heme group is hexa-coordinated, *i.e.*, two additional axial bonds are formed below and above the molecular plane of porphyrin macrocycle. We use the default harmonic bonding and dihedral potential in Charmm 27 for the Fe-N coordination bonding. In addition, to maintain the coordination geometry of Fe atom as the heme center, the angular potential of N-Fe-O (where O is the water oxygen) in Charmm 27 is adopted to represent the angular interaction of N-Fe-N and the equilibrium angle is set to be 180°. The calcium ions, which coordinate with proteins' amino residues, are included in the simulations and interact with proteins via van der Waals and electrostatic potentials. Initially, we relax the newly added residues by MD simulations in vacuum with a stepwise heating protocol from 60 K to 298.15 K. To remove the 'bad contacts' between the added residues and the rest, which lead to huge repulsion, only the added residues are relaxed while all the others are fixed at a low temperature. Subsequently, we

obtain the solvated protein structure by MD simulations in an aqueous environment with the TIPS3P water model.[54] To neutralize the system, Na^+ counter ions are added in both vacuum and solvation simulations.

The third step is to obtain the predicted structure of the MtrF-OmcA complex using a protein-docking program, ZDOCK (version 3.0.2).[40] As an input to the ZDOCK program, we use two PDB files for MtrF and OmcA, respectively, that are sampled from the MD simulations described above. ZDOCK predicts the structure of a protein-protein complex by treating each protein as a rigid body and docking them. The complex structures are scored using a combination of shape complementarity, electrostatics, and statistical potential terms. ZDOCK returns *N* top-ranked configurations according to the scoring as *N* PDB files labeled by the ranking (*N* is typically 2000).

Next, we use our C-RANK program to sub-select *M* biologically plausible complex candidates from the *N* ZDOCK outputs, where $M << N$, using two criteria: (1) the minimum inter-cytochrome heme-heme distance (edge-to-edge metric) should be less than 10 Å, to support rapid ET, and (2) the orientation of both proteins in the complex must be compatible with their lipophilic nature, allowing both N-terminus lipid binding sites to face a common plane that serves as proxy for the outer membrane.

In the ZDOCK rigid docking, the protein hydrogen atoms and the coordinated calcium ions have been ignored. Therefore, finally, these hydrogen atoms are re-added and calcium ions are re-positioned at original sites of both proteins according to their coordinated amino residues. Then the whole MtrF-OmcA complex is re-solvated with added counter ions following the stepwise heating protocol from 60 K to 298.18 K. After the heating, the complex is relaxed in the aqueous environment for 20 ns. The top candidates are now further screened by ranking the binding affinities based on the binding free energy calculated using the MM/PBSA method. For the

MM/PBSA calculation, we have modified the recently developed suite of Bash/Perl scripts, GMXPBSA 2.1,[44] which combines the Gromacs software[53] for the computation of protein-protein interaction energy from MD simulation and the Adaptive Poisson-Boltzmann Solver (APBS) program[55] for the estimation of solvation free energy in a continuum solvent medium. In MM/PBSA, the protein-protein binding free energy ($\Delta G_{binding}$) of A + B $\rightarrow$ AB is defined as the free energy difference between the complex (AB) and the sum of the free energies of the individual proteins (A and B) in aqueous environment as

$$\Delta G_{\ binding} = G_{aqu}^{AB} - G_{aqu}^{A} - G_{aqu}^{B}. \quad (1)$$

$\Delta G_{binding}$ is calculated with the thermodynamic cycle shown in Fig. 4 to include the complex solvation effect in the binding while minimizing the computational cost. In Fig. 4, ΔG_{gas} is the binding free energy for the AB complex in the gas phase, and (ΔG_{sol}^{i}) is the total solvation free energy for component *i* (*i* = A, B, or AB). Technical details are provided in Ref. 56, where we validated our MM/PBSA procedure for related systems.

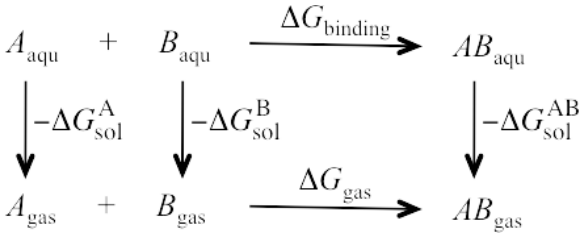

Fig. 4. Thermodynamic cycle to calculate the binding free energy of two proteins, A and B.

2.2. Divide-conquer-recombine kinetic Monte Carlo simulations of electron transfer

We performed KMC simulations[28-31] to study ET dynamics in the top-ranked MtrF-OmcA configurations selected. The KMC simulation[23] treats electron-hopping events in the MtrF-OmcA heme network with N_h (= 20) sites, where a heme site is labelled by index $i \in \{1,\ldots,N_h\}$. The i-th heme is either occupied by an electron (n_i = 1, corresponding to Fe^{2+}) or unoccupied (n_i = 0, corresponding to Fe^{3+}), where n_i is the electron occupation number of the i-th heme. The system is characterized by electron hopping rates k_{ij} between a pair (i, j) of adjacent heme sites, electron injection rate α into selected entrance heme, and electron-ejection rate β from a selected exit heme. As implemented previously,[23] we start the KMC simulation by emptying all sites and resetting the time to 0. At each KMC step, one of the following events occurs: (1) an electron is injected with rate α if the entrance heme is unoccupied; (2) an electron is ejected with rate β if the exit heme is occupied; or (3) an electron hops from heme i to one of its nearest-neighbour hemes j with rate k_{ij} if heme i is occupied and heme j is unoccupied. The probability of choosing a particular electron-hopping event is proportional to its specific hopping rate. This is implemented by choosing an event stochastically as follows: Let L be the total number of possible events and k_l (l = 1,...,L) be the rate of the l-th event; specific event l^* is chosen such that

$$\sum_{l=1}^{l^*-1} k_l < \xi_1 k_{\text{total}} < \sum_{l=1}^{l^*} k_l, \tag{2}$$

where ξ_1 is a random number uniformly distributed in the range (0,1) and

$$k_{\text{total}} = \sum_{l=1}^{L} k_l \tag{3}$$

is the cumulative rate of all possible events. We displace the electron involved in the chosen event and increment the time by $t = -\ln(\xi_2)/k_{\text{total}}$, where ξ_2 is another random number. KMC steps are

repeated for K (~10^6) times to describe the time evolution of the system until the system reaches a steady state. The time-averaged electron occupation density at heme i is calculated as

$$\langle n_i \rangle = \frac{\sum_{t=1}^{K} n_i(t)\tau(t)}{\sum_{t=1}^{K} \tau(t)}. \quad (4)$$

where $\tau(t)$ is the time increment and $n_i(t)$ is the electron occupation number of the i-th heme at the t-th KMC step. The overall electron occupation density $\langle n \rangle$ is given by an average over all heme sites. The steady-state current J is obtained by dividing the net number of injected electrons during K KMC steps by the total elapsed time $\sum_{t=1}^{K} \tau(t)$.

VizBET supports two options in computing the ET rates k_{ij}. In both options, a thermodynamic integration protocol[57] is needed to estimate the change of the Gibbs free energy ΔG_{ij} and the reorganization energy λ associated with the ET from heme sites i to j.[24, 58, 59] The two options differ in the way the electronic coupling H_{ij} for the ET reaction is computed. In the first-principles QM/MM option,[60, 61] a divide-conquer-recombine (DCR) algorithmic framework[25] is employed. Here, the divide-and-conquer (DC) phase computes H_{ij} for each heme pair using the QM/MM method, where each QM calculation employs DC density functional theory (DFT). The calculated ET rates are used in the recombination phase to synthesize global ET dynamics using KMC simulations as described above. According to the non-adiabatic rate equation, the rate of ET, k_{ij}, from the i-th heme to the j-th heme is expressed as[1]

$$k_{ij} = \frac{2\pi}{\hbar} \langle |H_{ij}|^2 \rangle \frac{1}{\sqrt{4\pi\lambda k_B T}} \exp\left(-\frac{(\Delta G_{ij} + \lambda)^2}{4\lambda k_B T} \right), \quad (5)$$

where T is the temperature, and $\hbar$ and k_B are the Planck and Boltzmann constants, respectively. To calculate inter-heme ET rates within a MtrF molecule, for example, Breuer *et al.*[24] estimated

the electronic coupling by using the QM/MM method and a variant of DCDFT called fragment-orbital density functional theory.

The second option to calculate k_{ij} employs a phenomenological form of the non-adiabatic rate-equation,[4]

$$k_{ij} = k_0 \exp\left(- \beta R_{ij} - \frac{(\Delta G_{ij} + \lambda)^2}{4\lambda k_B T} \right), \quad (6)$$

where R_{ij} is the edge-to-edge distance between hemes i and j, $k_0 = 10^{13}$ (s^{-1}), and β is a tunneling decay factor. Despite its simplicity, Eq. (6) correctly reflects the exponential decay of the tunneling probability and predicts ET rates in broad classes of biomolecules.[4]

2.3. Visualization of electron transfer

To animate the ET dynamics in DCR-KMC simulations, we have developed a plugin[62] to the VMD software.[21] VMD is a molecular visualization program for large biomolecular systems using 3D graphics and built-in scripting. Our plugin is implemented using the Tcl scripting language.[63] We have used VMD version 1.9.1.

Multiple time frames from the KMC simulation are saved as a multi-frame PDB file, in which the n_i value of each Fe atom is written in the temperature-factor (BETA) field in its ATOM record. The Tcl script copies the PDB-BETA values to the USER fields in the TRAJECTORY data category in VMD, so that the time variation of the n_i values can be animated as color changes according to one of the built-in color scales in VMD. The animation can be shown in a display window or can be saved as a sequence of image files to create a movie file. The Fe atoms are represented by spheres with color-coded electron occupation n_i. The Fe charge dynamics are overlaid with the NewCartoon representation in VMD of the protein complex. This animation is

used to examine the hopping of individual electrons within the heme network in the protein complex. Alternatively, VizBET can visualize the time averaged electron occupation,

$$\langle n_i \rangle_t = \frac{\sum_{s=1}^{t} n_i(s)t(s)}{\sum_{s=1}^{t} t(s)} \tag{7}$$

In this way, we can animate how the time-averaged electron distribution converges to a steady state.

2.4. Immersive visualization of electron transfer

Our iBET framework enhances the perceptual depth over that of VizBET by exporting the visual output into VR instead of a 2D computer monitor (Fig. 3). We selected the Oculus Rift as our commodity device.[35] The system consists of a HMD and a head-movement sensor (Fig. 5). The HMD provides a stereoscopic 3D perspective to the user by showing images from different view angles to the left and right eyes. The sensor tracks the movement of the user's head to recalculate the images accordingly. In addition, the user navigates in the 3D model using a mouse and a keyboard. Optionally, a gamepad can be used as an input device for navigation. Porting the molecular model to VR is enabled by the Unity game engine.[64] In Unity, objects in the 3D model are manipulated and animated using the C# programming language[65] and can subsequently be rendered in VR.

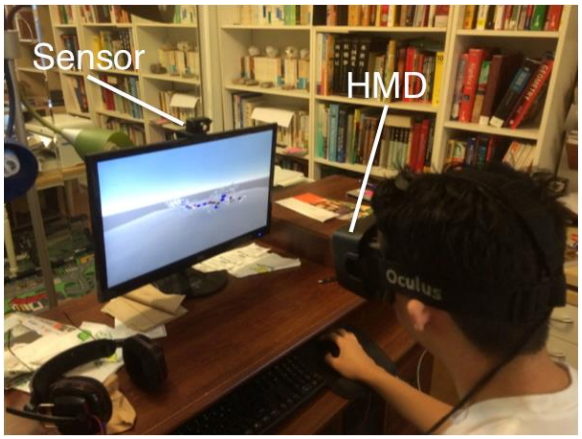

Fig. 5. iBET rendering of ET dynamics in a cytochrome complex in Oculus Rift.

Figure 6 is a screenshot of the ET dynamics in the heme network of a MtrF-OmcA cytochrome complex being animated from within Unity. The central image is a 2D representation of the 3D scene transmitted to the Oculus Rift HMD. The user uses a mouse to rotate the scene, and the W, S, A and D keys in a keyboard to move in the forward, backward, left, and right directions, respectively. In addition, the user can physically turn their heads to look around different

directions. The head-movement tracking system senses the movement and renders appropriate images. In this application, the occupation and un-occupation of each heme are represented by red and blue colors, respectively, of a sphere that represents Fe in the heme.

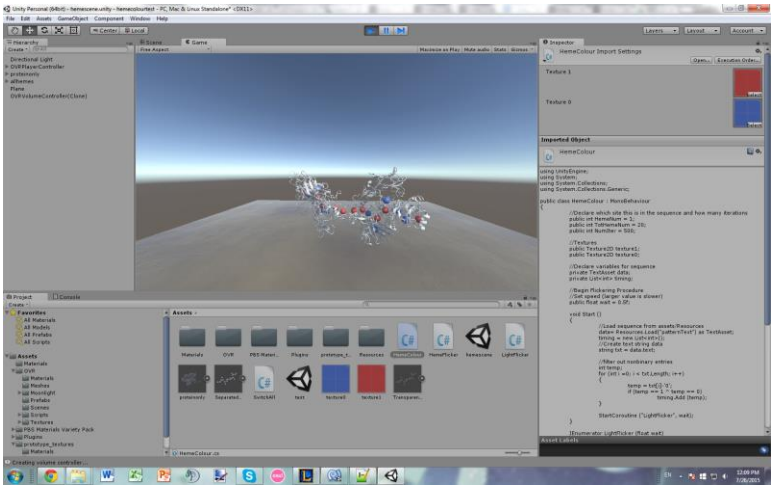

Fig. 6. Screenshot of the Unity game engine showing the cytochrome-complex data and Oculus control modules.

3. Results

To illustrate the use of VizBET/iBET, we study lateral ET parallel to the outer membrane across the top ranked configuration of the MtrF-OmcA complex, according to the ET and orientation criteria described above, shown in Fig. 7. Remarkably, this MtrF-OmcA configuration is arranged similarly to the OmcA dimer crystallized by Edwards *et al.*,[51] which is the only reported structure of two interacting decaheme cytochromes. This similarity further suggests that our screening procedure is capable of predicting biologically plausible structures of the complex. In this top ranked MtrF-OmcA configuration, heme 5 of each cytochrome serves as the site of

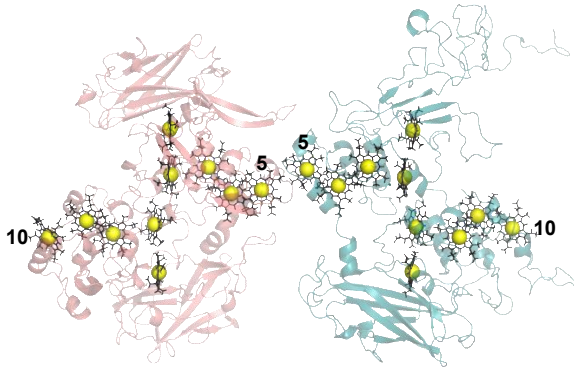

Fig. 7. The Top-ranked MtrF-OmcA configuration according to our ET and orientation criteria, showing the 20 heme arrangement within the complex. Hemes 5 of both proteins define the inter-cytochrome contact with a 5.58 Å edge-to-edge distance.

cytochrome-cytochrome interaction, linking the two proteins' long axes from heme 10 of one to heme 10 of the other.

3.1. Nonequilibrium phase transitions

A multistep ET process has been hypothesized to allow long-distance electron transport through multiple complexes along a bacterial nanowire.[13] To examine this hypothesis along our top ranked configuration, the ET rates within the MtrF-OmcA complex are obtained by parameterizing and generalizing the H_{ij}, ΔG_{ij}, and λ calculated in Ref. 24 for MtrF. The H_{ij} parameters throughout the complex were fit to a single exponential $\langle |H_{ij}|^2 \rangle^{1/2}(r) = A \exp[-\beta(r - r_o)/2]$, where r is the edge-to-edge distance between i and j, r_o = 3.6 Å, □ = 1.65 Å^{-1} and A = 3.77 meV, as presented in Ref. 24 for MtrF. Similarly, the ΔG_{ij}, and λ values computed for specific *i-j* pairs in MtrF are generalized throughout the whole combined MtrF-OmcA complex in our example.

Figure 8 shows the KMC simulation results. Here, we chose the injection site as heme 10 in MtrF, and the ejection site as heme 10 in OmcA. By varying the incoming (α) and outgoing (β) ET rates, our simulation reveals a rich phase diagram for the MtrF-OmcA complex in the α - β plane (Fig. 8a). Three distinct phases are observed in the time-averaged occupation density of the icosaheme complex, similar to those recently reported for the decaheme MtrF.[23] A low-density (LD) phase, where the hemes are mostly oxidized, is observed when transport is limited by ET from intercellular donor molecules ($\alpha < \beta$). A high-density (HD) phase, where the hemes are mostly reduced, is observed when transport is limited by ET to extracellular electron acceptors ($\alpha > \beta$). Finally, a 'maximum-current' (MC) phase is observed when both α and β exceed the smallest heme-to-heme ET rate within the complex, which is ~10^4 s^{-1} along the path.[24] The high electron

flux character of the MC phase, compared to the LD and HD phases, is easily identified in Fig. 8b, which presents the phase behavior of the electron flux in the α-β plane. Intriguingly, cellular respiration measurements and estimates of the cellular cytochrome content translate to ET rates up to 10^3 s^{-1} per outer-membrane cytochrome.[23] This rate is located near the triple junction between the three phases; it appears that life operates where a small change in the electrochemical environment triggers large bioelectronic responses. It should be noted that these nonequilibrium phase transitions are a direct consequence of electron-electron interactions,[66-68] which necessitate the use of many-body theory or simulations such as our KMC simulation.

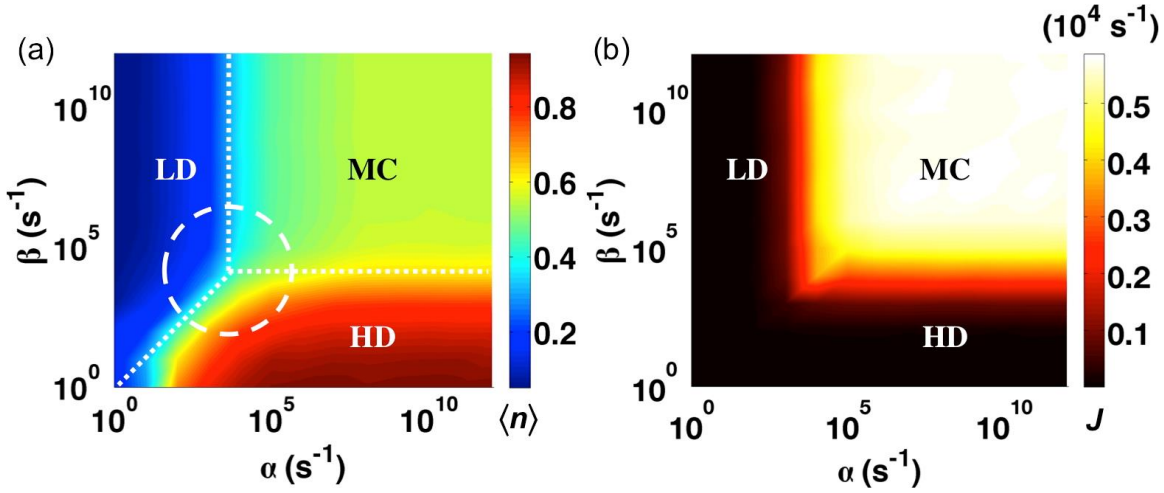

Fig. 8. (a) Phase diagram of the time-averaged electron occupation density $\langle n \rangle$ for all 20 hemes as a function of the incoming (α) and outgoing (β) ET rates. The white dotted lines delineate the low-density (LD), high-density (HD) and maximum current (MC) phases. The white dashed circle corresponds to experimentally estimated respiration rates. (b) The corresponding phase diagram of the net electron flux J.

3.2. Animation of electron-transfer dynamics

Figure 9a shows a snapshot of the animation of the above KMC simulations, where $\alpha = 10^5$ s^{-1} and $\beta = 10^5$ s^{-1}. Such a static representation does not necessarily capture the nature of the many-electron ET dynamics, which is essential for understanding the microscopic mechanisms underlying the nonequilibrium phase transitions. The animation capability of VizBET is expected to bring about such dynamic insight. Three supplementary movie files, S1.mov, S2.mov, and

S3.mov,[69] animate the ET dynamics corresponding to the LD ($\alpha = 10^2$ s^{-1} and $\beta = 10^5$ s^{-1}), HD ($\alpha = 10^5$ s^{-1} and $\beta = 10^2$ s^{-1}), and MC ($\alpha = 10^5$ s^{-1} and $\beta = 10^5$ s^{-1}) phases, respectively. Each movie depicts the final 500 KMC steps from a total of one million steps simulated. These movies show representative ET dynamics in a steady state in each phase after the initial transient well dies out. In the animation of the LD phase, a majority of the hemes are unoccupied, corresponding to the color blue. In the animation of the HD phase, a majority of the hemes are occupied, corresponding to the color red. Finally, in the MC phase, we observe extensive ET events, represented by more frequent and distributed color changes of the individual hemes. These movies help give insight into the possible roles and impact of individual hemes in the complex, for instance by identifying sites that act as carrier traps, or always reduced hemes which may act as electron donors to soluble acceptors capable of diffusing inside the complex.[23]

To highlight ET events, we augment the above animations by representing each event as a directed edge. Namely, an ET event between two Fe atoms is represented by a cylinder that connects the participating Fe atoms.

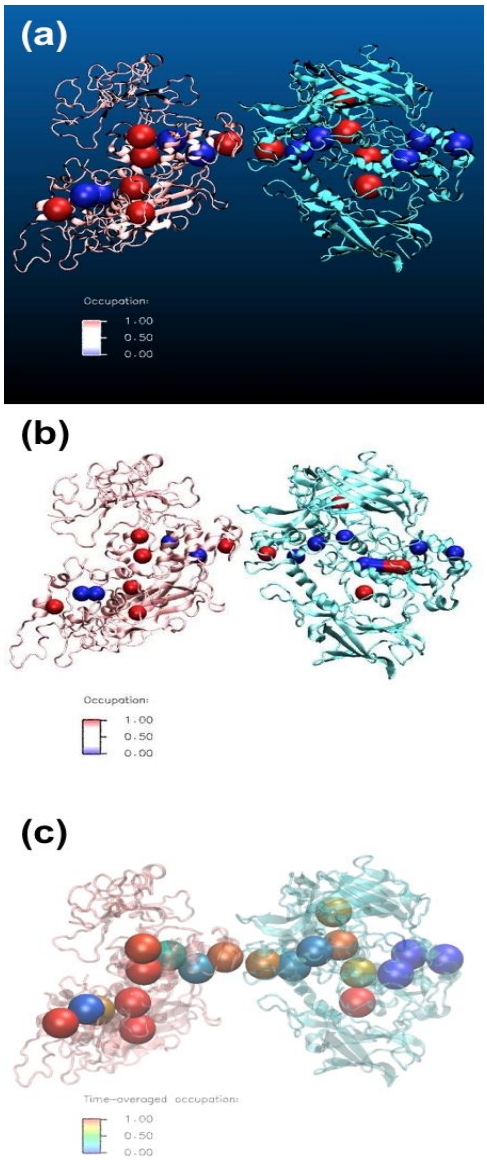

Fig. 9. Visualizing the KMC simulation of ET dynamics in the MtrF-OmcA complex. The Fe atoms are represented as spheres, and are overlaid with the NewCartoon representation of the entire protein complex, where MtrF and OmcA are represented in red and blue shades, respectively. Fe^{2+} and Fe^{3+} are represented by red and blue spheres, respectively. (a) A single snapshot from the final 500 KMC steps of the simulation. (b) A snapshot from the same simulation as (a), where an ET event is represented by a directed edge. (c) Time-averaged electron occupation, of each Fe atom (as defined by Eq. (13)). Injection/ejection parameters: $\alpha=\beta=10^5$ s^{-1}.

Here, one end of the cylinder attached to the source of ET is colored blue, while the other end connected to the destination of ET is colored red. Supplementary movie S4.mov animates ET events in the MC phase ($\alpha = 10^5$ s^{-1} and $\beta = 10^5$ s^{-1}). Figure 9b shows a snapshot of this animation.

As an alternative to the above movies, VizBET outputs the color-coded time-averaged electron occupation of each Fe atom as defined by Eq. (7). Figure 9c shows such representation of the time-averaged occupation animation. This representation allows the user to see how the distribution of time-averaged occupation approaches a steady state distribution as time progresses. Supplementary movie S5.mov animates time evolution of the time-averaged electron occupation in the MC phase ($\alpha = 10^5$ s^{-1} and $\beta = 10^5$ s^{-1}) for the initial 10,000 KMC steps.

4. Discussion

In this report, we have described a computational framework named VizBET and its immersive extension iBET to visualize biological ET dynamics in VR. We have presented VizBET/iBET using an outer-membrane MtrF-OmcA cytochrome complex in *Shewanella oneidensis* MR-1 as an example. Such spatiotemporal data visualizations and analyses[70] are expected to provide valuable insight into the microscopic mechanisms of ET processes in not only biological but also other novel nanostructures such as dislocation-mediated metallic nanowires in ceramics.[71, 72] In particular, our results shed useful light on boosting the efficiency of *Shewanella*-based microbial fuel cells[73] by increasing the ET rate. These microbial fuel cells can simultaneously produce electric power and fresh water from wastewater toward solving the global energy and environmental problems. Furthermore, genetically engineered bacteria could help fight climate change by reducing CO_2 faster than wild bacterial species do.[74]

References

1. R. A. Marcus and N. Sutin, "Electron transfers in chemistry and biology", Biochim Biophys Acta **811**, 265-322 (1985).
2. D. N. Beratan, J. N. Betts and J. N. Onuchic, "Protein electron-transfer rates set by the bridging secondary and tertiary structure", Science **252**, 1285-1288 (1991).
3. C. C. Moser, J. M. Keske, K. Warncke, R. S. Farid and P. L. Dutton, "Nature of biological electron-transfer", Nature **355**, 796-802 (1992).
4. H. B. Gray and J. R. Winkler, "Electron tunneling through proteins", Q Rev Biophys **36**, 341-372 (2003).
5. J. P. Lin, I. A. Balabin and D. N. Beratan, "The nature of aqueous tunneling pathways between electron-transfer proteins", Science **310**, 1311-1313 (2005).
6. C. R. Myers and K. H. Nealson, "Bacterial Manganese Reduction and Growth with Manganese Oxide as the Sole Electron-Acceptor", Science **240**, 1319-1321 (1988).
7. J. K. Fredrickson, M. F. Romine, A. S. Beliaev, J. M. Auchtung, M. E. Driscoll, T. S. Gardner, K. H. Nealson, A. L. Osterman, G. Pinchuk, J. L. Reed, D. A. Rodionov, J. L. M. Rodrigues, D. A. Saffarini, M. H. Serres, A. M. Spormann, I. B. Zhulin and J. M. Tiedje, "Towards environmental systems biology of Shewanella", Nat Rev Microbiol **6**, 592-603 (2008).
8. M. Y. El-Naggar and S. E. Finkel, "Live Wires", Scientist **27**, 38-43 (2013).
9. M. Breuer, K. M. Rosso, J. Blumberger and J. N. Butt, "Multi-haem cytochromes in Shewanella oneidensis MR-1: structures, functions and opportunities", J Royal Soc Interface **12** (2015).

10. Y. A. Gorby, S. Yanina, J. S. McLean, K. M. Rosso, D. Moyles, A. Dohnalkova, T. J. Beveridge, I. S. Chang, B. H. Kim, K. S. Kim, D. E. Culley, S. B. Reed, M. F. Romine, D. A. Saffarini, E. A. Hill, L. Shi, D. A. Elias, D. W. Kennedy, G. Pinchuk, K. Watanabe, S. Ishii, B. Logan, K. H. Nealson and J. K. Fredrickson, "Electrically conductive bacterial nanowires produced by Shewanella oneidensis strain MR-1 and other microorganisms", P Natl Acad Sci USA **103**, 11358-11363 (2006).

11. M. Y. El-Naggar, G. Wanger, K. M. Leung, T. D. Yuzvinsky, G. Southam, J. Yang, W. M. Lau, K. H. Nealson and Y. A. Gorby, "Electrical transport along bacterial nanowires from Shewanella oneidensis MR-1", P Natl Acad Sci USA **107**, 18127-18131 (2010).

12. K. M. Leung, G. Wanger, M. Y. El-Naggar, Y. Gorby, G. Southam, W. M. Lau and J. Yang, "Shewanella oneidensis MR-1 bacterial nanowires exhibit p-type, tunable electronic behavior", Nano Lett **13**, 2407-2411 (2013).

13. S. Pirbadian, S. E. Barchinger, K. M. Leung, H. S. Byun, Y. Jangir, R. A. Bouhenni, S. B. Reed, M. F. Romine, D. A. Saffarini, L. Shi, Y. A. Gorby, J. H. Golbeck and M. Y. El-Naggar, "Shewanella oneidensis MR-1 nanowires are outer membrane and periplasmic extensions of the extracellular electron transport components", P Natl Acad Sci USA **111**, 12883-12888 (2014).

14. C. R. Myers and J. M. Myers, "Localization of cytochromes to the outer-membrane of anaerobically grown Shewanella-putrefaciens MR-1", J Bacteriol **174**, 3429-3438 (1992).

15. C. R. Myers and J. M. Myers, "Cell surface exposure of the outer membrane cytochromes of Shewanella oneidensis MR-1", Lett Appl Microbiol **37**, 254-258 (2003).

16. B. H. Lower, R. Yongsunthon, L. Shi, L. Wildling, H. J. Gruber, N. S. Wigginton, C. L. Reardon, G. E. Pinchuk, T. C. Droubay, J. F. Boily and S. K. Lower, "Antibody recognition

force microscopy shows that outer membrane cytochromes OmcA and MtrC are expressed on the exterior surface of Shewanella oneidensis MR-1", Appl Environ Microb **75**, 2931-2935 (2009).

17. D. J. Richardson, J. N. Butt, J. K. Fredrickson, J. M. Zachara, L. Shi, M. J. Edwards, G. White, N. Baiden, A. J. Gates, S. J. Marritt and T. A. Clarke, "The porin-cytochrome' model for microbe-to-mineral electron transfer", Mol Microbiol **85**, 201-212 (2012).
18. L. Shi, B. W. Chen, Z. M. Wang, D. A. Elias, M. U. Mayer, Y. A. Gorby, S. Ni, B. H. Lower, D. W. Kennedy, D. S. Wunschel, H. M. Mottaz, M. J. Marshall, E. A. Hill, A. S. Beliaev, J. M. Zachara, J. K. Fredrickson and T. C. Squier, "Isolation of a high-affinity functional protein complex between OmcA and MtrC: two outer membrane decaheme c-type cytochromes of Shewanella oneidensis MR-1", J Bacteriol **188**, 4705-4714 (2006).
19. C. Bucking, F. Popp, S. Kerzenmacher and J. Gescher, "Involvement and specificity of Shewanella oneidensis outer membrane cytochromes in the reduction of soluble and solid-phase terminal electron acceptors", FEMS Microbiol Lett **306**, 144-151 (2010).
20. B. E. Logan, "Exoelectrogenic bacteria that power microbial fuel cells", Nat Rev Microbiol **7**, 375-381 (2009).
21. W. Humphrey, A. Dalke and K. Schulten, "VMD: Visual molecular dynamics", J Mol Graph Modell **14**, 33-38 (1996).
22. I. A. Balabin, X. Q. Hu and D. N. Beratan, "Exploring biological electron transfer pathway dynamics with the Pathways plugin for VMD", J Comput Chem **33**, 906-910 (2012).
23. H. S. Byun, S. Pirbadian, A. Nakano, L. Shi and M. Y. El-Naggar, "Kinetic Monte Carlo simulations and molecular conductance measurements of the bacterial decaheme cytochrome MtrF", ChemElectroChem **1**, 1932-1939 (2014).

24. M. Breuer, K. M. Rosso and J. Blumberger, "Electron flow in multiheme bacterial cytochromes is a balancing act between heme electronic interaction and redox potentials", P Natl Acad Sci USA **111**, 611-616 (2014).

25. F. Shimojo, R. K. Kalia, M. Kunaseth, A. Nakano, K. Nomura, S. Ohmura, K. Shimamura and P. Vashishta, "A divide-conquer-recombine algorithmic paradigm for multiscale materials modeling", J Chem Phys **140**, 18A529 (2014).

26. A. Warshel and M. Levitt, "Theoretical studies of enzymic reactions: dielectric, electrostatic and steric stabilization of the carbonium ion in the reaction of lysozyme", J Mol Biol **103**, 227-249 (1976).

27. A. I. Krylov and P. M. W. Gill, "Q-Chem: an engine for innovation", Rev Comput Mol Sci **3**, 317-326 (2013).

28. A. B. Bortz, M. H. Kalos and J. L. Lebowitz, "New algorithm for Monte Carlo simulation of Ising spin systems", J Comput Phys **17**, 10-18 (1975).

29. D. T. Gillespie, "General method for numerically simulating stochastic time evolution of coupled chemical-reactions", J Comput Phys **22**, 403-434 (1976).

30. K. A. Fichthorn and W. H. Weinberg, "Theoretical foundations of dynamic Monte Carlo simulations", J Chem Phys **95**, 1090-1096 (1991).

31. A. F. Voter, in *Radiation Effects in Solids*, edited by K. E. Sickafus, E. A. Kotomin and B. P. Uberuaga (Springer, Dordrecht, The Netherlands, 2006).

32. **Competition Entrant**, H. S. Byun, H. Ma, T. Wei and M. Y. El-Naggar, "A framework for stochastic simulations and visualization of biological electron-transfer dynamics", Comput Phys Commun **193**, 1-9 (2015).

33. H. Rheingold, *Virtual Reality: Exploring the Brave New Technologies* (Summit Books, New York, NY, 1991).

34. I. E. Sutherland, "A head-mounted three dimensional display", P Am Fed Info Process Soc Conf, AFIPS **I**, 757-764 (ACM, 1968).

35. B. A. Davis, K. Bryla and P. A. Benton, *Oculus Rift in Action* (Manning Publications, Shelter Island, NY, 2015).

36. H. J. Li, K. S. Leung, T. Nakane and M. H. Wong, "iView: an interactive WebGL visualizer for protein-ligand complex", BMC Bioinfo **15**, 56 (2014).

37. **Competition Entrant**, E. Moen, H. S. Byun, H. Ma, B. Newman, A. McDowell, T. Wei and M. Y. El-Naggar, "iBET: immersive visualization of biological electron-transfer dynamics", Comput Phys Commun, submitted (2015).

38. H. M. Berman, J. Westbrook, Z. Feng, G. Gilliland, T. N. Bhat, H. Weissig, I. N. Shindyalov and P. E. Bourne, "The Protein Data Bank", Nucl Acids Res **28**, 235-242 (2000).

39. A. Roy, A. Kucukural and Y. Zhang, "I-TASSER: a unified platform for automated protein structure and function prediction", Nat Protoc **5**, 725-738 (2010).

40. B. G. Pierce, K. Wiehe, H. Hwang, B. H. Kim, T. Vreven and Z. P. Weng, "ZDOCK server: interactive docking prediction of protein-protein complexes and symmetric multimers", Bioinfo **30**, 1771-1773 (2014).

41. J. Srinivasan, T. E. Cheatham, P. Cieplak, P. A. Kollman and D. A. Case, "Continuum solvent studies of the stability of DNA, RNA, and phosphoramidate - DNA helices", J Am Chem Soc **120**, 9401-9409 (1998).

42. I. Massova and P. A. Kollman, "Computational alanine scanning to probe protein-protein interactions: A novel approach to evaluate binding free energies", J Am Chem Soc **121**, 8133-8143 (1999).

43. C. Paissoni, D. Spiliotopoulos, G. Musco and A. Spitaleri, "GMXPBSA 2.0: A GROMACS tool to perform MM/PBSA and computational alanine scanning", Comput Phys Commun **185**, 2920-2929 (2014).

44. C. Paissoni, D. Spiliotopoulos, G. Musco and A. Spitaleri, "GMXPBSA 2.1: A GROMACS tool to perform MM/PBSA and computational alanine scanning", Comput Phys Commun **186**, 105-107 (2015).

45. C. Newham, *Learning the bash Shell: Unix Shell Programming* (O'Reilly Media, Sebastopol, CA, 2005).

46. R. L. Henderson, "Job scheduling under the Portable Batch System", Lec Notes Comp Sci **949**, 279-294 (1995).

47. J. M. Wozniak, T. G. Armstrong, M. Wilde, D. S. Katz, E. Lusk and I. T. Foster, "Swift/T: Scalable data flow programming for many-task applications", ACM SIGPLAN Notices **48**, 309-310 (2013).

48. E. Deelman, J. Blythe, Y. Gil, C. Kesselman, G. Mehta, S. Patil, M. H. Su, K. Vahi and M. Livny, "Pegasus: mapping scientific workflows onto the Grid", Grid Comput **3165**, 11-20 (2004).

49. http://www.ncbi.nlm.nih.gov/.

50. T. A. Clarke, M. J. Edwards, A. J. Gates, A. Hall, G. F. White, J. Bradley, C. L. Reardon, L. Shi, A. S. Beliaev, M. J. Marshall, Z. M. Wang, N. J. Watmough, J. K. Fredrickson, J.

M. Zachara, J. N. Butt and D. J. Richardson, "Structure of a bacterial cell surface decaheme electron conduit", P Natl Acad Sci USA **108**, 9384-9389 (2011).

51. M. J. Edwards, N. A. Baiden, A. Johs, S. J. Tomanicek, L. Y. Liang, L. Shi, J. K. Fredrickson, J. M. Zachara, A. J. Gates, J. N. Butt, D. J. Richardson and T. A. Clarke, "The X-ray crystal structure of Shewanella oneidensis OmcA reveals new insight at the microbe-mineral interface", FEBS Lett **588**, 1886-1890 (2014).

52. V. N. Maiorov and G. M. Crippen, "Size-independent comparison of protein 3-dimensional structures", Proteins **22**, 273-283 (1995).

53. B. Hess, C. Kutzner, D. van der Spoel and E. Lindahl, "GROMACS 4: Algorithms for highly efficient, load-balanced, and scalable molecular simulation", J Chem Theory Comput **4**, 435-447 (2008).

54. A. D. MacKerell, D. Bashford, M. Bellott, R. L. Dunbrack, J. D. Evanseck, M. J. Field, S. Fischer, J. Gao, H. Guo, S. Ha, D. Joseph-McCarthy, L. Kuchnir, K. Kuczera, F. T. K. Lau, C. Mattos, S. Michnick, T. Ngo, D. T. Nguyen, B. Prodhom, W. E. Reiher, B. Roux, M. Schlenkrich, J. C. Smith, R. Stote, J. Straub, M. Watanabe, J. Wiorkiewicz-Kuczera, D. Yin and M. Karplus, "All-atom empirical potential for molecular modeling and dynamics studies of proteins", J Phys Chem B **102**, 3586-3616 (1998).

55. N. A. Baker, D. Sept, S. Joseph, M. J. Holst and J. A. McCammon, "Electrostatics of nanosystems: Application to microtubules and the ribosome", P Natl Acad Sci USA **98**, 10037-10041 (2001).

56. **Competition Entrant**, H. Ma and T. Wei, "Study of lysozyme mobility and binding free energy during adsorption on a graphene surface", Appl Phys Lett **106**, 153701 (2015).

57. V. A. Ngo, "Parallel-pulling protocol for free-energy evaluation", Phys Rev E **85**, 036702 (2012).

58. M. Breuer, P. Zarzycki, J. Blumberger and K. M. Rosso, "Thermodynamics of Electron Flow in the Bacterial Deca-heme Cytochrome MtrF", J Am Chem Soc **134**, 9868-9871 (2012).

59. M. Breuer, P. Zarzycki, L. Shi, T. A. Clarke, M. J. Edwards, J. N. Butt, D. J. Richardson, J. K. Fredrickson, J. M. Zachara, J. Blumberger and K. M. Rosso, "Molecular structure and free energy landscape for electron transport in the decahaem cytochrome MtrF", Biochem Soc T **40**, 1198-U1158 (2012).

60. A. Warshel and M. Karplus, "Calculation of ground and excited-state potential surfaces of conjugated molecules. 1. formulation and parametrization", J Am Chem Soc **94**, 5612-5625 (1972).

61. A. Warshel and M. Levitt, "Theoretical studies of enzymic reactions - dielectric, electrostatic and steric stabilization of carbonium-ion in reaction of lysozyme", J Mol Biol **103**, 227-249 (1976).

62. http://www.ks.uiuc.edu/Research/vmd/script_library/.

63. J. K. Ousterhout and K. Jones, *Tcl and the Tk Toolkit*, Second ed. (Addison-Wesley, Boston, MA, 2009).

64. W. Goldstone, *Unity 3.x Game Development Essentials*, 2nd ed. (Packt Publishing, Birmingham, UK, 2011).

65. J. Albahari and B. Albahari, *C# 5.0 in a Nutshell* (O'Reilly, Sebastopol, CA, 2012).

66. I. Neri, N. Kern and A. Parmeggiani, "Totally asymmetric simple exclusion process on networks", Phys Rev Lett **107**, 068702 (2011).

67. T. Chou, K. Mallick and R. K. P. Zia, "Non-equilibrium statistical mechanics: from a paradigmatic model to biological transport", Rep Prog Phys **74**, 116601 (2011).

68. M. Gorissen, A. Lazarescu, K. Mallick and C. Vanderzande, "Exact current statistics of the asymmetric simple exclusion process with open boundaries", Phy Rev Lett **109**, 170601 (2012).

69. Supplementary movies are found at:

S1.mov:

http://www.sciencedirect.com/science/MiamiMultiMediaURL/1-s2.0-S0010465515001083/1-s2.0-S0010465515001083-mmc1.mp4/271575/html/S0010465515001083/c7ecaeb46c7ffc94b2373110e42a22db/mmc1.mp4

S2.mov:

http://www.sciencedirect.com/science/MiamiMultiMediaURL/1-s2.0-S0010465515001083/1-s2.0-S0010465515001083-mmc2.mp4/271575/html/S0010465515001083/350c5c64438ba4660aca87026db43967/mmc2.mp4

S3.mov:

http://www.sciencedirect.com/science/MiamiMultiMediaURL/1-s2.0-S0010465515001083/1-s2.0-S0010465515001083-mmc3.mp4/271575/html/S0010465515001083/d206eba0aa26ae477c236f66cdc8e4ab/mmc3.mp4

S4.mov:

http://www.sciencedirect.com/science/MiamiMultiMediaURL/1-s2.0-S0010465515001083/1-s2.0-S0010465515001083-mmc4.mp4/271575/html/S0010465515001083/f3cc0c0037825f5b7fb82817ff6d66a2/mmc4.mp4

S5.mov:

http://www.sciencedirect.com/science/MiamiMultiMediaURL/1-s2.0-S0010465515001083/1-s2.0-S0010465515001083-mmc5.mp4/271575/html/S0010465515001083/1234e14f9493efa784a8fff61c131506/mmc5.mp4

70. D. Bhattarai and B. B. Karki, "Atomistic visualization: Space-time multiresolution integration of data analysis and rendering", J Mol Graph Modell **27**, 951-968 (2009).

71. A. Nakamura, K. Matsunaga, J. Tohma, T. Yamamoto and Y. Ikuhara, "Conducting nanowires in insulating ceramics", Nat Mater **2**, 453-456 (2003).

72. K. Tsuruta, E. Tochigi, Y. Kezuka, K. Takata, N. Shibata, A. Nakamura and Y. Ikuhara, "Core structure and dissociation energetics of basal edge dislocation in alpha-Al_2O_3: a combined atomistic simulation and transmission electron microscopy analysis", Acta Mater **65**, 76-84 (2014).

73. C. Shubert, "Circuits of slime", Nature **441**, 277-279 (2006).

74. K. Krieger, Genetically engineered bacteria could help fight climate change, Science News, Feb. 26, 2012; http://news.sciencemag.org/2012/02/genetically-engineered-bacteria-could-help-fight-climate-change.